The activated state of a sodium channel voltage sensor in a membrane environment

Sudha Chakrapani[a], Pornthep Sompornpisut[b], Pathumwadee Intharathep[b], Benoît Roux[a], and Eduardo Perozo[a,1]

[a]Department of Biochemistry and Molecular Biology, University of Chicago, Center for Integrative Science, 929 East 57th Street, Chicago, IL 60637; [b]Computational Chemistry Unit Cell, Department of Chemistry, Faculty of Science, Chulalongkorn University, 254 Phayathai Road, Bangkok 10330, Thailand

Edited by Ramón Latorre, Centro de Neurociencias, Universidad de Valparaíso, Valparaíso, Chile, and approved January 29, 2010 (received for review December 9, 2009)

Direct structural insights on the fundamental mechanisms of permeation, selectivity, and gating remain unavailable for the Na^+ and Ca^{2+} channel families. Here, we report the spectroscopic structural characterization of the isolated Voltage-Sensor Domain (VSD) of the prokaryotic Na^+ channel NaChBac in a lipid bilayer. Site-directed spin-labeling and EPR spectroscopy were carried out for 118 mutants covering all of the VSD. EPR environmental data were used to unambiguously assign the secondary structure elements, define membrane insertion limits, and evaluate the activated conformation of the isolated-VSD in the membrane using restrain-driven molecular dynamics simulations. The overall three-dimensional fold of the NaChBac-VSD closely mirrors those seen in KvAP, Kv1.2, Kv1.2-2.1 chimera, and MlotiK1. However, in comparison to the membrane-embedded KvAP-VSD, the structural dynamics of the NaChBac-VSD reveals a much tighter helix packing, with subtle differences in the local environment of the gating charges and their interaction with the rest of the protein. Using cell complementation assays we show that the NaChBac-VSD can provide a conduit to the transport of ions in the resting or "down" conformation, a feature consistent with our EPR water accessibility measurements in the activated or "up" conformation. These results suggest that the overall architecture of VSD's is remarkably conserved among K^+ and Na^+ channels and that pathways for gating-pore currents may be intrinsic to most voltage-sensors. Cell complementation assays also provide information about the putative location of the gating charges in the "down/resting" state and hence a glimpse of the extent of conformational changes during activation.

complementation assays | EPR spectroscopy | gating charges | electrical excitability

Voltage-gated Na^+ channels (Na_v) orchestrate the rapid movement of Na^+ across the membrane that govern the rising phase of action potential in nerve and muscle cells. Eukaryotic Na_vs are composed of a single polypeptidic chain forming four homologous domains, each composed of six transmembrane (TM) helices. NaChBac, a prokaryotic voltage-gated Na_v from *Bacillus halodurans* (1) is the simplest member of this family, consisting of four identical 6TM-subunits resembling the individual domains of the eukaryotic Na_v and Ca_v channels. Although both activation and inactivation gating kinetics in NaChBac are significantly slower than in eukaryotic Na_v, its steep voltage-dependent activation and Na^+ selective permeation properties firmly place this channel within the Na_v family (1–3). The functional behavior of voltage-gated channels in general relies on the energetic coupling between the voltage-sensor domain (VSD), formed by the TM segments S1–S4, and the pore domain (PD), formed by the segments S5–S6. However there is ample evidence that supports the structural independence of the two domains. The VSD from *Shaker* channel when transferred to nonvoltage sensitive potassium channel confers voltage-dependent gating (4, 5). Mackinnon and colleagues showed that the isolated-VSD of KvAP could be stably expressed in detergent (6). Our own work confirmed that this domain can not only remain monomeric in a membrane environment (7), but that its three-dimensional architecture was almost completely unaltered when compared to that in the full-length channel (8). More recently, the discovery of voltage-sensor phosphatases (Ci-VSP) (9) and voltage-gated proton channels (Hv) (10, 11) has revealed that VSDs are not exclusive to ion channels with canonical PDs. In fact, they can be coupled to control enzymatic activity, as in Ci-VSP, or even serve as scaffold for ion permeation as found in Hv channels (12). In addition, features such as hysteresis of voltage-dependence, a property widely studied in many voltage-gated channels such as the Na_v (13), K_v (14), and HCN channels (15, 16) are now known to be intrinsically associated to the VSD (17, 18). These results suggest that the isolated-VSD is a meaningful functional modular unit that can serve as a basic model system for structural and dynamical studies aimed at discovering the general principles of voltage sensing.

Here, we have determined the three-dimensional architecture of the isolated-VSD of NaChBac in a near-native environment using site-directed spin-labeling and EPR spectroscopy. This information was used to evaluate atomic models of NaChBac-VSD through restrained molecular dynamics (MD) simulations incorporating solvent accessibility values as experimental restraints (19). This model is compared with the crystal structures of the VSD of KvAP and Kv1.2-2.1 chimera (6, 20) and demonstrates that the general structural principles and basic functional properties of VSD domains are conserved across K^+ and Na^+ channels.

Results and Discussion

The purified NaChBac isolated-VSD (Fig. S1*A*) in decylmaltoside (DM) runs as a monodisperse monomer in gel filtration chromatography, with an elution volume of 14.2 mL and an absolute molecular mass of $\sim 22 \pm 4$ kDa, as determined from light scattering/refractive index analysis (Fig. S1*B*). The mutant T110C in the S3–S4 linker was chosen to assay the aggregation of the sensor on the membranes by FRET using fluorescein-maleimide and tetramethylrhodamine-maleimide as transfer pair (7, 8, 21). We found that the isolated-sensor remains monodisperse in all of the tested reconstituted membrane systems (Fig. S1*C*).

Probing the Three-Dimensional Architecture of NaChBac-VSD by EPR Spectroscopy. To evaluate the molecular architecture of the VSD in a membrane environment, 118 cysteine mutants covering most of the isolated-VSD (16-137) were purified, spin-labeled, and reconstituted in 1-palmitoyl-2-oleoyl-sn-glycero-3-phospho-

Author contributions: S.C. and E.P. designed research; S.C. and P.I. performed research; P.S. and B.R. contributed new reagents/analytic tools; S.C., P.S., and E.P. analyzed data; and S.C. and E.P. wrote the paper.

The authors declare no conflict of interest.

This article is a PNAS Direct Submission.

[1]To whom correspondence should be addressed. E-mail: eperozo@uchicago.edu.

This article contains supporting information online at www.pnas.org/cgi/content/full/0914109107/DCSupplemental.

choline (POPC): 1-palmitoyl-2-oleoyl-sn-glycero-3-phospho-(1'-rac-glycerol) (POPG) mixture (3:1, mol:mol). All measurements were made in the absence of membrane potential, so presumably the vast majority of the spin-labeled sensors populate the "up-state" or activated conformation (7, 8). Our analyses were centered on two types of dynamic EPR structural information (22–27): First, estimations of the spin-probe motional freedom from the inverse of the central line width of the first derivative absorption spectra (ΔH_o^{-1}). Second, spin-probe solvent accessibility evaluated by collisional relaxation methods. Here, nonpolar molecular oxygen (ΠO_2) serves as a contrast agent to evaluate membrane exposure while polar Ni(II) ethylenediaminediacetic acid (ΠNiEdda) reports the extent of aqueous exposure.

Analysis of the complete spectral dataset for the isolated-VSD is shown in Fig. 1*A*. Probe mobility (ΔH_o^{-1}, *black*) and O_2 accessibility (ΠO_2, *red*) show clear periodic behavior in each of the TM segments, compatible with an α-helical structure (data amplitude changes every third or fourth residue). Further, the ΠO_2 values in each of the TM segments are seen to peak towards the middle of the helix (indicated by the *bent arrows*), consistent with high O_2 levels in the center of the bilayer. The location of the putative loop regions are clearly marked by large excursion in both ΔH_o^{-1} and ΠNiEdda which also allows for an unambiguous assignment of the boundaries for the TM segments. Together these data clearly reflect a transmembrane orientation of the isolated-VSD. A closer inspection at the periodic variation of the EPR data shows that while S1 and S2 are nearly continuous, a break in the ΠO_2 pattern is apparent in S3 and S4 (marked by *arrows*) which might be reflective of a bending or kinking of the α-helix. A break in S4 periodicity was also observed in lanthanide resonance energy transfer (LRET) measurements of NaChBac full-length channel (28). It is interesting to note that most positions corresponding to conserved residues within the VSD families show low ΠO_2 (*green asterisks* in Fig. 1*A*) and hence predicted to point into the core of the helical bundle. The relative orientations of the helices with respect to each other and the membrane lipids can be predicted based on the direction of the calculated ΠO_2 moment (*black arrow*), as shown on a helical wheel representation (Fig. 1*B*).

The Conformation of the S4 Segment. The ΠNiEdda values of the S3–S4 loop point to the start of the S4 helix at residue 110, one helical turn above the first arginine R113 (R1). Examination of ΠO_2 reveals that the S4 segment is not a simple α-helix; residues 110-119 show low values every third-forth positions while for residues 120-128 it is every third position (Fig. 2*A*). The derived power spectra of the N-terminal half of S4 shows a distinct peak centered at 99.8° reflecting its α-helical nature while the C-terminal end reveals a peak at 118.1° which is characteristic of a 3_{10} helix. The 3_{10} periodicity of the S4 helix terminates below Pro128 and suggests that this residue forms the start of the S4-S5 linker. The occurrence of a 3_{10} helical hydrogen-bonding pattern in S4 was observed in MlotiK channels and in the K1.2-2.1 chimera (20, 29), but not in the KvAP sensor crystal structure (6) or in the EPR accessibility parameters of the KvAP sensor in the membrane (7, 8). One structural advantage of a 3_{10} helical conformation for S4 is that the series of charged arginines (1 every 3 residues) can be made to point toward a water-filled crevice at the center of the VSD core, which is more favorable energetically (20). An α-helix-to-3_{10} transition might allow S4 to stretch and spring back, changing the position of the gating charges within the electric field, as previously suggested (20).

Although the topology of the VSDs in KvAP and the Kv1.2-2.1 chimera are essentially superimposable (20), the S4 arginines show significant differences in their immediate environments. In the KvAP structure R1 and R2 are positioned on the membrane-exposed face of S4; R3 is exposed to a mixed membrane-water environment; while R4, R5, and K6 clearly point into the VSD (6). Our EPR data of KvAP was consistent with this orientation, as R1 and R2 show clear O_2 exposure, which gradually decreases as we move from R3 towards K6 (7, 8). In Kv1.2, R1-R4 are positioned in similar environments as those

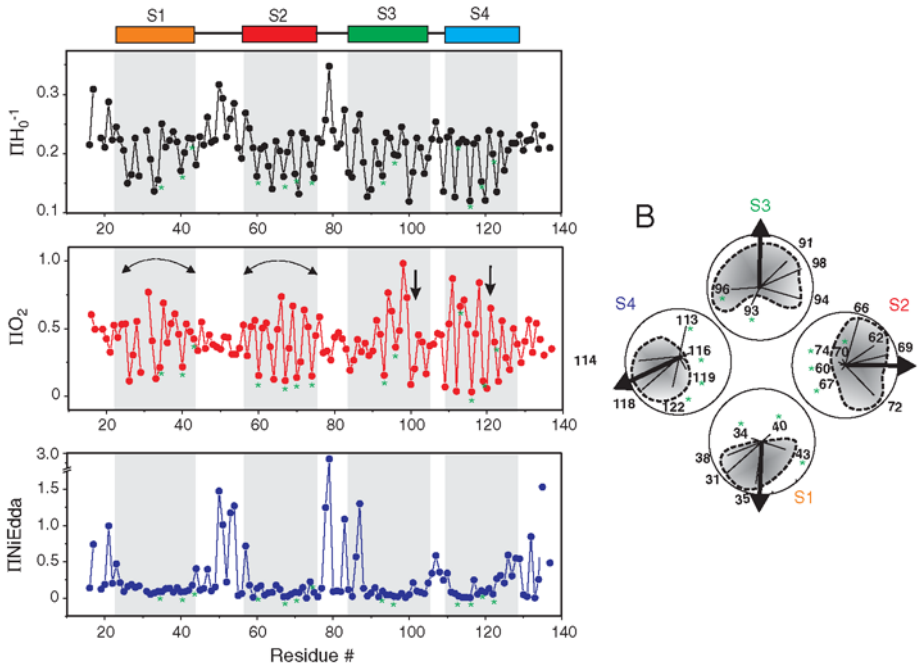

Fig. 1. EPR based structural analysis of the isolated-VSD. (*A*) Mobility ΔH_0^{-1} (*black*), O_2 accessibility ΠO_2 (*red*) and NiEdda accessibility ΠNiEdda (*blue*). The *gray* regions represent the putative TM segments from the hydropathy plot. *Green asterisks* denote highly conserved residues with VSDs. *Bent arrows* point to the increase in ΠO_2 towards the center of the bilayer in S1 and S2 and *straight arrows* indicate a break in helix periodicity in S3 and S4. (*B*) Helical wheel representation of ΠO_2 superimposed in a polar coordinate representation. The relative orientation of the helices can be predicated based on the direction of the resultant vector, which points towards the lipid facing phase of the helix. The *shaded* area within the *dashed lines* highlights the degree of eccentricity for the complete set of accessibility data relative to the maximal accessibility vector.

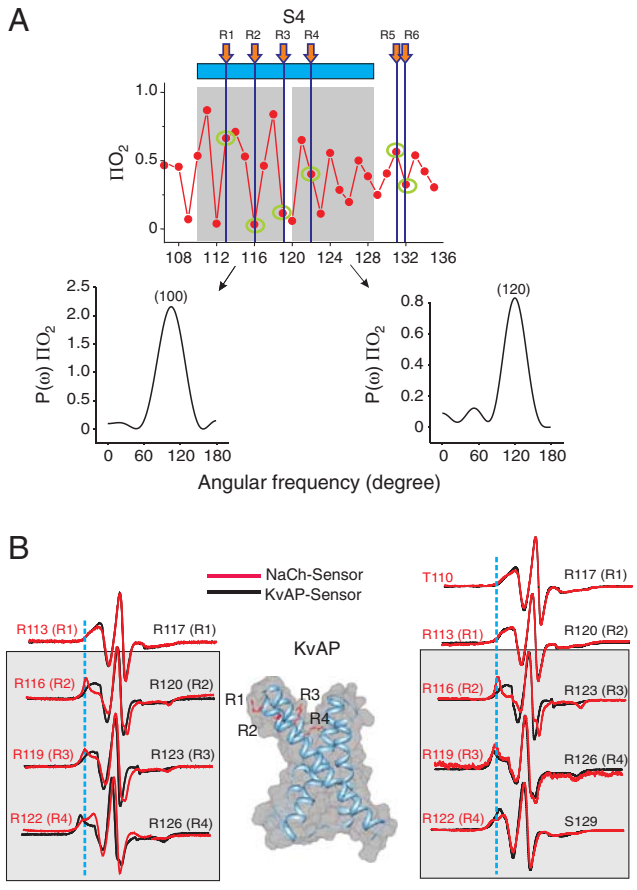

Fig. 2. Environment of the S4 segment (*A*) Profile of changes in the ΠO_2 parameters reflects a break in periodicity. Fourier transform power spectra of ΠO_2 shows that the peak angular frequency occurs at ~99.8° for the upper-half of S4 corresponding to an α-helix, while it is at ~118.1° for the lower-half suggesting a 3_{10} helical structure. (*B*) An overlap of representative X-band CW-EPR spectra of spin-labeled mutants at corresponding arginines in S4 for the VSD from NaChBac (*red*) and KvAP (*black*). *Blue line* shows the location of immobile component of the spectra (*Left*). Position of arginine side-chains as seen in the crystal structure of the isolated-VSD of KvAP (*center*). An overlap of EPR spectra of the corresponding positions based on the alignment of NaChBac and KvAP VSDs (*Right*). The shaded boxes highlight positions that show maximal change in line shape.

seen in KvAP (30). In the Kv1.2-2.1 chimera, however, R0 is exposed to the membrane interface, R1 faces a mixed environment while R2-R6 point towards S1 and S2 helices (20). Fig. 2*B* shows a comparison of the spectral line-shapes for NaChBac-VSD spin-labeled at the equivalent gating charges with those in the isolated-KvAP-VSD. Both the spectra at R1, as well as the accessibility to O_2 are essentially identical, suggesting that the Arg at this position is likely to be at the membrane interface and able to interact favorably with the phosphate head groups of the lipids (20, 31, 32). However, Positions R2 and R3 show a much higher degree of immobilization in NaChBac-VSD, suggesting that they point into the VSD core as seen in the Kv1.2-2.1 chimera rather than in KvAP. At R4 the spin-probe is more mobile in NaChBac-VSD than in KvAP which, together with the observed ΠNiEdda in residues immediately below, might suggests that R4 could be positioned near the interface connecting the inner and outer cavities in the up-state. In general, interfacial arginines show lower apparent ΠNiEdda (7, 8). The differences in the environment of Arg side-chains in KvAP and NaChBac could occur as a consequence of the position of arginines on the S4 helix as reflected by the sequence alignment (Fig. S1*A*). An overlap based on this alignment (Fig. 2*B*, *right*) shows a better match of the spectral line shapes, although in comparison NaChBac spectra is more immobile at R2 and R3.

Key arginines in the S4 segment are known to be stabilized by a network of salt-bridge interactions with acidic residues in S1, S2, and S3 transmembrane segments (33–36). These interactions presumably stabilize S4 arginines in the low dielectric environment on the membrane. As seen with the R2-R3 positions, the spin-label at these positions (D60, E70, and D93) in NaChBac reports a more restricted dynamics in comparison to KvAP (Fig. S2*A* and *B*).

Water-Filled Crevices and Pathway for Gating-Pore Currents. Cysteine reactivity measurements first suggested the presence of water vestibules within VSDs (37–45). X-ray structures (6, 20, 30) show that bending of S3 away from the VSD core creates deep crevices at the center of the S1–S4 helical bundle that can be penetrated by water. ΠNiEdda of spin probes at positions lining these crevices confirms the presence of aqueous pathway within the VSD on the membrane (7, 8). Penetration of water molecules from either side of the VSD has been observed in MD simulations (32, 43–45). The VSD aqueous pathway/cavity has been implicated in playing a critical role in reducing the effective thickness of the bilayer around the S4 charges and thereby facilitating the focusing of membrane electric field. This feature obliterates the requirement of large S4 movement during activation (46–48).

In NaChBac-VSD, ΠNiEdda in S3 reveals that there are only 14 residues that show little or no water exposure (Fig. 3*A* and *B*). In this case, the hydrophobic region of the membrane approaches an apparent "thickness" of <20 Å in the vicinity of the S3 segment. The aqueous accessibility of crevices measured by the collisional quenching of NiEdda, is usually an underestimation of the actual penetration depth (7, 8). A decrease in ΠO_2 in the C-terminal half of S3 (Fig. 1) along with the high motional freedom of residues above Gly 100 suggest that water penetration is favored by the bending introduced by the glycine residue. This position is analogous to Pro99 in KvAP (6) and Pro265 in the

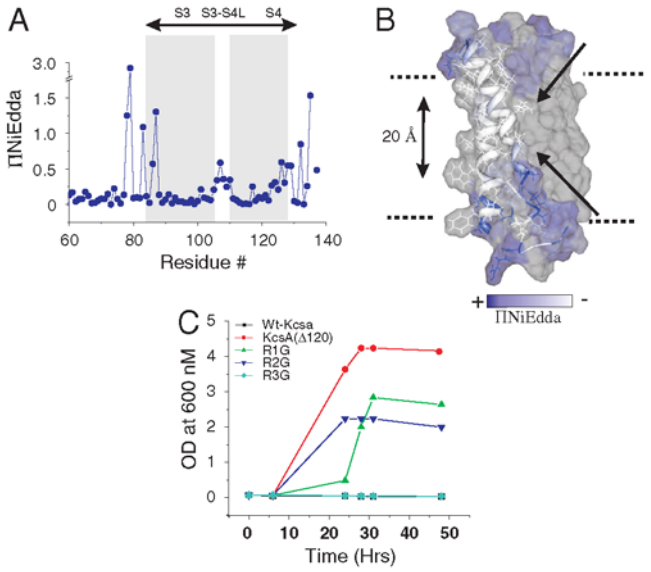

Fig. 3. Aqueous crevices within the VSD. (*A*) ΠNiEdda values for the residues comprising the S3–S4 segment in the isolated-VSD. (*B*) ΠNiEdda values mapped on the S3 segment of the NaChBac-VSD model to show the depth of water accessible areas (*blue arrows*) within the transmembrane region of the protein. The *dotted line* denotes the putative limits of the membrane. (*C*) LB2003 complementation assay. Mutant strain LB2003 transformed with Gly mutants at R1 (*green triangles*), R2 (*blue inverted triangles*), and R3 (*cyan diamonds*), the negative control is closed wt-KcsA (*black squares*) and the positive control is the C-terminal truncated KcsA (Δ120) (*red circles*).

Kv1.2-2.1 chimera (20). It is interesting to note that this position is occupied by proline or glycine, in voltage-gated ion channel families (49–54) and serine or threonine in the Hv channel (10, 11) and VSP families (9). All of these residues have been suggested to destabilize α-helix. Therefore formation of crevices by the bending of S3 appears to be a common property of VSDs.

Another structural difference among VSDs is centered on the helix kink at the S3 segment. In KvAP, the S3 segment is seen to be partially unwound below the Pro99 (6), reflected as a loss of periodicity in this region in the EPR measurements of the full-length channel and the isolated-VSD of KvAP (7, 8). In the Kv1.2 structure, S3 appears as a single helix with a bending at the Pro265, although the resolution is limited. A similar bending at Pro265 is also seen in the Kv1.2-2.1 chimera (20). In NaChBac-VSD, the S3a region is strongly α-helical and shows significantly less exposure to water than that seen in KvAP, suggesting that the tilting of the S3b and hence the depth of the cleft may not be as well defined as in KvAP.

The presence of an aqueous channel in the VSD interior represents a potential pathway for the passage of protons and other cations across the membrane. Such gating-pore mediated ion permeation has been shown to occur in the up-state of the sensor through mutations at R3 and R4 (46, 55, 56) and in the down-state by mutating R1 and R2 (57, 58). We evaluated the presence of such a pathway in the NaChBac-VSD in its down-state by carrying out in vivo complementation experiments using the *Escherichia coli* mutant LB2003 (59). This mutant lacks all K^+ uptake systems (kup1, ΔkdpABC5, ΔtrkA) and requires high extracellular K^+ concentrations to grow. We used C-terminal truncated KcsA (Δ120), which has a faulty lower gate and allows finite K^+ permeation, as our positive control (60). LB2003 cells were able to grow in low K^+ medium when expressing NaChBac-VSD mutants with Gly at R1 and R2, with mutation R2G most effective in cell growth complementation, suggesting that R2 (and to some extent R1) line the pathway connecting the internal and external vestibule in the down-state (Fig. 3*C*). Glycine substitution at R3, on the other hand, was unable to complement the K^+ deficiency and was indistinguishable from our negative control (closed wt-KcsA). Finding from these results are twofold: First, the isolated-VSD can by itself support gating-pore currents; Second, the side-chains of R1 and R2 act as a barrier between the internal and external vestibule in the core of the down-state of the VSD. This later interpretation is further supported by the observation that in the Na_v channels, mutations of the R1 and R2 in the S4 segment of domain II cause gating-pore current in the down state (57).

Refining a Structural Model for the NaChBac-VSD. The present set of structural data has been used as constrains for the refinement of a three-dimensional atomic model of the membrane-embedded NaChBac-VSD in its activated state. In this recently developed Pseudoatom-Driven Solvent Accessibility Refinement method (PaDSAR) the solvent accessibility restraints from EPR measurements were incorporated into the MD simulations (*SI Text*) (19). The refined mobility and accessibility data satisfies the mobility and accessibility measurements (Fig. 4). This three-dimensional atomic model has remarkable similarities with the known Kv channel sensors in terms of the overall fold and conserved interactions (6, 20, 30). However in comparison to the isolated-VSD of KvAP, the packing of TM helices in this model appears to be much tighter with differences in the S4 topology and the location of gating charges.

We then probed the stability of this atomic model using all-atom MD simulation in an explicit hydrated membrane environment. The average rmsd of the VSD backbone relative to the initial model is 3.5 Å for the VSD (Fig. S3*A*). During 10 ns simulations the overall packing of the helices remained intact, an observation that we have taken as indicative of the structural

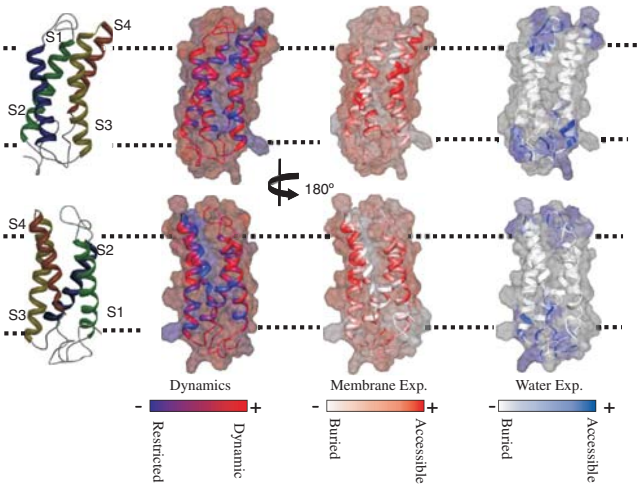

Fig. 4. A model of the activated state of the NaCh-VSD obtained from EPR-based refinement. Mobility parameter (ΔH_o^{-1}), O_2 accessibility parameter (ΠO_2) and NiEdda accessibility parameters (ΠNiEdda) are mapped on to a surface representation of the model.

stability of our model. The structure was essentially unaltered during 10 ns of free dynamics with no restraints (either EPR or secondary structural restraints). Water molecules were seen to spontaneously diffuse from both the extracellular and intracellular end of the VSD and were occluded around residues R3/R4 and D60 forming an hour-glass shaped water profile such that these residues lie at the interface connecting the two cavities (Fig. 5*A* and *B*). The extent of water penetration during MD simulations suggests that the crevices determined by EPR are an underestimation of the actual depths seen on the membrane. This is not unexpected, given the volume of the aqueous contrast agent NiEdda. Water penetration has also been seen in MD simulations of the VSD of KvAP and Kv1.2 (43, 44). At the end of the 10 ns trajectory all the S4 arginines were well solvated by water molecules, with R1 and R2 found to interact with the lipid head-group and water molecules (Fig. S3*C*). This lipid-S4 interaction was first proposed due to the apparent requirement of phosphate head-group of the membrane lipids for proper voltage-dependent activation (31). Other MD simulations have also shown specific interactions between the arginine side-chains and the lipid phosphate groups in Kv1.2 channels (32). Further, our MD simulations showed that R3 formed stable salt-bridges interactions with D60 at S2 (Fig. 5*C*, Fig. S3*B*), Similar interaction has been proposed in Shaker based on second-site charge-reversal mutations (36). This interaction is also in agreement with recent studies in NaChBac in which Cys at D60 and R3 form spontaneous cross-linking upon activation (61).

Fundamental to elucidating the mechanism of voltage-dependent activation is the understanding of the extent of gating-charge movement with the membrane field. Gating currents measurements in NaChBac suggests a displacement of ~4 elementary charges per subunit across the membrane field during activation, roughly similar to that measured for *Shaker* and Kv2.1. This would mean that all four arginines in S4 contribute to gating by moving from an interior to an exterior position in relation to the transmembrane voltage field. Indeed, our results from extensive EPR analysis and MD simulations of the "up/activated" state, together with cell complementation assays of the "down/resting" state of the VSD, provide clues to the extent of movement of S4 during voltage activation in NaChBac. In the "up/activated" state, our model is consistent with a conformation of the VSD where R1–R4 face the external cleft accessible from the outside, with R3 and R4 positioned in the narrowest region connecting the inward and outward-facing vestibules, while in the "down/resting" state, S4 rearranges so that R1 and R2 are able to

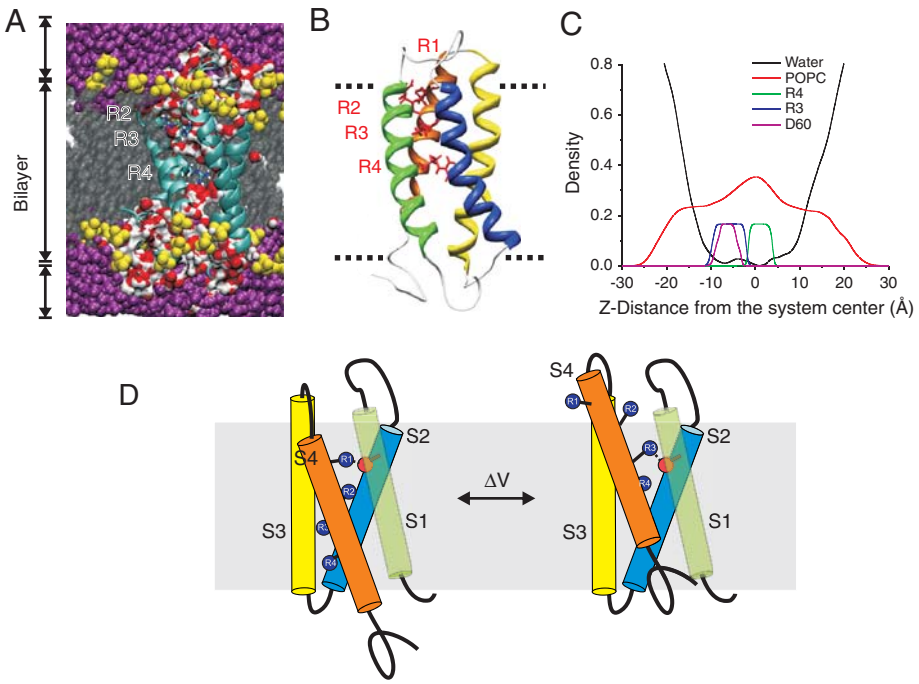

Fig. 5. All-atom MD simulations of the EPR based model of NaChbac-VSD (*A*) A snapshot of the system embedded in membrane and water. *Red* and *white* surface was rendered for water molecules. R2, R3, and R4 side-chains are shown in *stick* representation. (*B*) EPR based model of NaChBac-VSD showing the location of gating arginines. (*C*) Density profiles for R3, D60, R4, lipid, and water during the last 5 ns of the free MD simulation. For clarification, 20 times magnification of the graphs has been applied for the three residues. (*D*) The putative "up" and "down" states of the NaChBac-VSD

bridge these two water-filled crevasses. Therefore, the most parsimonious model of activation in NaChBac would involve the movement of R4 to roughly the position occupied by R1 in the down/resting state (Fig. 5*D*). This finding is consistent with gating models presented for NaChBac gating (62) and for Kv1.2 (63). It is becoming increasingly evident that most VSDs sense voltage based on a common structural blueprint (6, 20, 29) and that any structural differences lie predominantly in the detailed arrangement and interaction of individual gating charges as well as in the overall dynamics that set the energetic requirements for the movement of the S3–S4 segments relative to the rest of the VSD. These subtle variations are likely to underlie the known heterogeneity in voltage-sensing among the large family of voltage-dependent cationic channels.

Materials and Methods

Protein Expression, Purification, and Spin-Labeling. The NaChBac isolated-VSD was expressed in *E.Coli* SG-13 cells. The protein was purified from isolated membranes in decylmaltoside, labeled with methanethiosulfonate spin-probe, and reconstituted in POPC:POPG lipid mixture (8).

EPR Spectroscopy and Analysis. We obtained X-band continuous wave (CW) EPR spectra from spin-labeled and reconstituted channels as described (23, 64, 65), using a Bruker EMX spectrometer equipped with a loop-gap resonator under the following conditions: 2 mW incident power, 100 kHz modulation frequency, and 1 G modulation amplitude. To estimate the periodic behavior of a given residue-specific enviromental parameter, a discrete Fourier transform power spectrum, P(ω), of the amino acid segment is calculated as a function of the angle between two adjacent side-chains (ω) (66, 67).

LB2003 Complementation Assay. LB2003 cells (59) carrying KcsA and NaChBac Gly mutants were grown at 37 °C overnight in 5 mL LB medium with 1% glucose, and 200 $\mu g\,mL^{-1}$ ampicillin. The cells were sedimented at 2300 × *g* for 5 min. The pellet was resuspended in 5 mL of minimal media (with 10 mM K^+) and sedimented again. After three cycles of washing the OD_{600} of each sample was adjusted to 0.075 with the above media. The cells were induced with 1 mM IPTG and the growth monitored at 37 °C.

Model Building and Refinement. Structure refinement was performed using the previously developed method, pseudoatom-driven solvent accessibility refinement (PaDSAR) incorporated in the CHARMM program version c32a2. This model was subsequently inserted into a preequilibrated POPC lipid bilayer. The MD simulations were carried out using CHARMM c32a2 with the all-atoms PARAM27 force fields for protein, lipid, water, and ion (68).

ACKNOWLEDGMENTS. We thank V. Jogini, L. Cuello, and V. Vásquez for insightful discussions; and H. Raghuraman, for critical reading and comments on the manuscript. This work was supported by National Institutes of Health Grants GM057846 (to E.P.); American Heart Association Postdoctoral Fellowship (to S.C.); and Rachadapisek Sompoch Endowment Fund (Chulalongkorn University) (to P.S.).

1. Ren D, et al. (2001) A prokaryotic voltage-gated sodium channel. *Science* 294(5550): 2372–2375.
2. Kuzmenkin A, Bezanilla F, Correa AM (2004) Gating of the bacterial sodium channel, NaChBac: Voltage-dependent charge movement and gating currents. *J Gen Physiol* 124(4):349–356.
3. Chahine M, Pilote S, Pouliot V, Takami H, Sato C (2004) Role of arginine residues on the S4 segment of the Bacillus halodurans Na+ channel in voltage-sensing. *J Membr Biol* 201(1):9–24.
4. Lu Z, Klem AM, Ramu Y (2001) Ion conduction pore is conserved among potassium channels. *Nature* 413(6858):809–813.
5. Lu Z, Klem AM, Ramu Y (2002) Coupling between voltage sensors and activation gate in voltage-gated K^+ channels. *J Gen Physiol* 120(5):663–676.
6. Jiang Y, et al. (2003) X-ray structure of a voltage-dependent K^+ channel. *Nature* 423(6935):33–41.
7. Chakrapani S, Cuello LG, Cortes DM, Perozo E (2008) Structural Dynamics of an isolated voltage-sensor domain in a lipid bilayer. *Structure* 16(3):398–409.
8. Cuello LG, Cortes DM, Perozo E (2004) Molecular architecture of the KvAP voltage-dependent K^+ channel in a lipid bilayer. *Science* 306(5695):491–495.
9. Murata Y, Iwasaki H, Sasaki M, Inaba K, Okamura Y (2005) Phosphoinositide phosphatase activity coupled to an intrinsic voltage sensor. *Nature* 435(7046):1239–1243.
10. Sasaki M, Takagi M, Okamura Y (2006) A voltage sensor-domain protein is a voltage-gated proton channel. *Science* 312(5773):589–592.
11. Ramsey IS, Moran MM, Chong JA, Clapham DE (2006) A voltage-gated proton-selective channel lacking the pore domain. *Nature* 440(7088):1213–1216.
12. Lee SY, Letts JA, MacKinnon R (2009) Functional reconstitution of purified human Hv1 H^+ channels. *J Mol Biol* 387(5):1055–1060.
13. Bezanilla F, Taylor RE, Fernandez JM (1982) Distribution and kinetics of membrane dielectric polarization. 1. Long-term inactivation of gating currents.. *J Gen Physiol* 79(1):21–40.

14. Larsson HP, Elinder F (2000) A conserved glutamate is important for slow inactivation in K^+ channels. *Neuron* 27(3):573–583.
15. Mannikko R, Pandey S, Larsson HP, Elinder F (2005) Hysteresis in the voltage dependence of HCN channels: Conversion between two modes affects pacemaker properties. *J Gen Physiol* 125(3):305–326.
16. Bruening-Wright A, Larsson HP (2007) Slow conformational changes of the voltage sensor during the mode shift in hyperpolarization-activated cyclic-nucleotide-gated channels. *J Neurosci* 27(2):270–278.
17. Villalba-Galea CA, Sandtner W, Starace DM, Bezanilla F (2008) S4-based voltage sensors have three major conformations. *Proc Natl Acad Sci USA* 105(46):17600–17607.
18. Villalba-Galea CA, et al. (2009) Charge movement of a voltage-sensitive fluorescent protein. *Biophys J* 96(2):L19–21.
19. Sompornpisut P, Roux B, Perozo E (2008) Structural refinement of membrane proteins by restrained molecular dynamics and solvent accessibility data. *Biophys J* 95(11):5349–5361.
20. Long SB, Tao X, Campbell EB, MacKinnon R (2007) Atomic structure of a voltage-dependent K^+ channel in a lipid membrane-like environment. *Nature* 450(7168): 376–382.
21. Vasquez V, Cortes DM, Furukawa H, Perozo E (2007) An optimized purification and reconstitution method for the MscS channel: Strategies for spectroscopical analysis. *Biochemistry* 46(23):6766–6773.
22. Altenbach C, Marti T, Khorana HG, Hubbell WL (1990) Transmembrane protein structure: Spin labeling of bacteriorhodopsin mutants. *Science* 248(4959):1088–1092.
23. Farahbakhsh ZT, Altenbach C, Hubbell WL (1992) Spin labeled cysteines as sensors for protein-lipid interaction and conformation in rhodopsin. *Photochem Photobiol* 56(6):1019–1033.
24. Altenbach C, Greenhalgh DA, Khorana HG, Hubbell WL (1994) A collision gradient method to determine the immersion depth of nitroxides in lipid bilayers: Application to spin-labeled mutants of bacteriorhodopsin. *Proc Natl Acad Sci USA* 91(5):1667–1671.
25. Hubbell WL, McHaourab HS, Altenbach C, Lietzow MA (1996) Watching proteins move using site-directed spin labeling. *Structure* 4(7):779–783.
26. Hubbell WL, Cafiso DS, Altenbach C (2000) Identifying conformational changes with site-directed spin labeling. *Nat Struct Biol* 7(9):735–739.
27. Altenbach C, Froncisz W, Hemker R, McHaourab H, Hubbell WL (2005) Accessibility of nitroxide side chains: Absolute Heisenberg exchange rates from power saturation EPR. *Biophys J* 89(3):2103–2112.
28. Richardson J, et al. (2006) Distance measurements reveal a common topology of prokaryotic voltage-gated ion channels in the lipid bilayer. *Proc Natl Acad Sci USA* 103(43):15865–15870.
29. Clayton GM, Altieri S, Heginbotham L, Unger VM, Morais-Cabral JH (2008) Structure of the transmembrane regions of a bacterial cyclic nucleotide-regulated channel. *Proc Natl Acad Sci USA* 105(5):1511–1515.
30. Long SB, Campbell EB, Mackinnon R (2005) Voltage sensor of Kv1.2: Structural basis of electromechanical coupling. *Science* 309(5736):903–908.
31. Schmidt D, Jiang QX, MacKinnon R (2006) Phospholipids and the origin of cationic gating charges in voltage sensors. *Nature* 444(7120):775–779.
32. Jogini V, Roux B (2007) Dynamics of the Kv1.2 voltage-gated K^+ channel in a membrane environment. *Biophys J* 93(9):3070–3082.
33. Papazian DM, et al. (1995) Electrostatic interactions of S4 voltage sensor in Shaker K^+ channel. *Neuron* 14(6):1293–1301.
34. Seoh SA, Sigg D, Papazian DM, Bezanilla F (1996) Voltage-sensing residues in the S2 and S4 segments of the Shaker K^+ channel. *Neuron* 16(6):1159–1167.
35. Planells-Cases R, Ferrer-Montiel AV, Patten CD, Montal M (1995) Mutation of conserved negatively charged residues in the S2 and S3 transmembrane segments of a mammalian K^+ channel selectively modulates channel gating. *Proc Natl Acad Sci USA* 92(20):9422–9426.
36. Tiwari-Woodruff SK, Schulteis CT, Mock AF, Papazian DM (1997) Electrostatic interactions between transmembrane segments mediate folding of Shaker K^+ channel subunits. *Biophys J* 72(4):1489–1500.
37. Larsson HP, Baker OS, Dhillon DS, Isacoff EY (1996) Transmembrane movement of the Shaker K^+ channel S4. *Neuron* 16(2):387–397.
38. Mannuzzu LM, Moronne MM, Isacoff EY (1996) Direct physical measure of conformational rearrangement underlying potassium channel gating. *Science* 271(5246):213–216.
39. Yang N, George AL, Jr, Horn R (1996) Molecular basis of charge movement in voltage-gated sodium channels. *Neuron* 16(1):113–122.
40. Cha A, Bezanilla F (1997) Characterizing voltage-dependent conformational changes in the Shaker K^+ channel with fluorescence. *Neuron* 19(5):1127–1140.
41. Sorensen JB, Cha A, Latorre R, Rosenman E, Bezanilla F (2000) Deletion of the S3-S4 linker in the Shaker potassium channel reveals two quenching groups near the outside of S4. *J Gen Physiol* 115(2):209–222.
42. Islas LD, Sigworth FJ (2001) Electrostatics and the gating pore of Shaker potassium channels. *J Gen Physiol* 117(1):69–89.
43. Treptow W, Tarek M (2006) Environment of the gating charges in the Kv1.2 Shaker potassium channel. *Biophys J* 90(9):L64–66.
44. Freites JA, Tobias DJ, White SH (2006) A voltage-sensor water pore. *Biophys J* 91(11): L90–92.
45. Sands ZA, Sansom MS (2007) How does a voltage sensor interact with a lipid bilayer? Simulations of a potassium channel domain. *Structure* 15(2):235–244.
46. Starace DM, Bezanilla F (2004) A proton pore in a potassium channel voltage sensor reveals a focused electric field. *Nature* 427(6974):548–553.
47. Ahern CA, Horn R (2005) Focused electric field across the voltage sensor of potassium channels. *Neuron* 48(1):25–29.
48. Chanda B, Asamoah OK, Blunck R, Roux B, Bezanilla F (2005) Gating charge displacement in voltage-gated ion channels involves limited transmembrane movement. *Nature* 436(7052):852–856.
49. Gray TM, Matthews BW (1984) Intrahelical hydrogen bonding of serine, threonine, and cysteine residues within alpha-helices and its relevance to membrane-bound proteins. *J Mol Biol* 175(1):75–81.
50. Blaber M, Zhang XJ, Matthews BW (1993) Structural basis of amino acid alpha helix propensity. *Science* 260(5114):1637–1640.
51. MacArthur MW, Thornton JM (1991) Influence of proline residues on protein conformation. *J Mol Biol* 218(2):397–412.
52. Monne M, Nilsson I, Elofsson A, von Heijne G (1999) Turns in transmembrane helices: Determination of the minimal length of a "helical hairpin" and derivation of a fine-grained turn propensity scale. *J Mol Biol* 293(4):807–814.
53. Ballesteros JA, Deupi X, Olivella M, Haaksma EE, Pardo L (2000) Serine and threonine residues bend alpha-helices in the $\mathrm{chi}(1) = \mathrm{g}(-)$ conformation. *Biophys J* 79(5):2754–2760.
54. Li-Smerin Y, Swartz KJ (2001) Helical structure of the COOH terminus of S3 and its contribution to the gating modifier toxin receptor in voltage-gated ion channels. *J Gen Physiol* 117(3):205–218.
55. Starace DM, Bezanilla F (2001) Histidine scanning mutagenesis of basic residues of the S4 segment of the Shaker K^+ channel. *J Gen Physiol* 117(5):469–490.
56. Sokolov S, Scheuer T, Catterall WA (2008) Depolarization-activated gating pore current conducted by mutant sodium channels in potassium-sensitive normokalemic periodic paralysis. *Proc Natl Acad Sci USA* 105(50):19980–19985.
57. Sokolov S, Scheuer T, Catterall WA (2007) Gating pore current in an inherited ion channelopathy. *Nature* 446(7131):76–78.
58. Tombola F, Pathak MM, Isacoff EY (2005) Voltage-sensing arginines in a potassium channel permeate and occlude cation-selective pores. *Neuron* 45(3):379–388.
59. Stumpe S, Bakker EP (1997) Requirement of a large K^+-uptake capacity and of extracytoplasmic protease activity for protamine resistance of *Escherichia coli*. *Arch Microbiol* 167(2/3):126–136.
60. Cortes DM, Cuello LG, Perozo E (2001) Molecular architecture of full-length KcsA: Role of cytoplasmic domains in ion permeation and activation gating. *J Gen Physiol* 117(2):165–180.
61. DeCaen PG, Yarov-Yarovoy V, Zhao Y, Scheuer T, Catterall WA (2008) Disulfide locking a sodium channel voltage sensor reveals ion pair formation during activation. *Proc Natl Acad Sci USA* 105(39):15142–15147.
62. Shafrir Y, Durell SR, Guy HR (2008) Models of voltage-dependent conformational changes in NaChBac channels. *Biophys J* 95(8):3663–3676.
63. Pathak MM, et al. (2007) Closing in on the resting state of the Shaker K^+ channel. *Neuron* 56(1):124–140.
64. Gross A, Hubbell WL (2002) Identification of protein side chains near the membrane-aqueous interface: A site-directed spin labeling study of KcsA. *Biochemistry* 41(4): 1123–1128.
65. Perozo E, Cortes DM, Cuello LG (1998) Three-dimensional architecture and gating mechanism of a K^+ channel studied by EPR spectroscopy. *Nat Struct Biol* 5(6):459–469.
66. Donnelly D, Overington JP, Blundell TL (1994) The prediction and orientation of alpha-helices from sequence alignments: The combined use of environment-dependent substitution tables, Fourier transform methods and helix capping rules. *Protein Eng* 7(5):645–653.
67. Cornette JL, et al. (1987) Hydrophobicity scales and computational techniques for detecting amphipathic structures in proteins. *J Mol Biol* 195(3):659–685.
68. MacKerell ADJ, et al. (1998) All-atom empirical potential for molecular modeling and dynamics studies of proteins. *J Phys Chem B* 102(18):3586–3616.